



## Article

# Enhancing Image Quality via Robust Noise Filtering Using Redescending M-Estimators

Ángel Arturo Rendón-Castro <sup>1</sup>, Dante Mújica-Vargas <sup>1,\*</sup>, Antonio Luna-Álvarez <sup>1</sup>  
and Jean Marie Vianney Kinani <sup>2</sup>

<sup>1</sup> Department of Computer Science, Tecnológico Nacional de México/CENIDET, Interior Internado Palmira S/N, Palmira, Cuernavaca 62490, Mexico; angel.rendon18ce@cenidet.edu.mx (Á.A.R.-C.)

<sup>2</sup> Unidad Profesional Interdisciplinaria de Ingeniería Campus Hidalgo, Instituto Politécnico Nacional, Pachuca 07738, Mexico

\* Correspondence: dante.mv@cenidet.tecnm.mx

**Abstract:** In the field of image processing, noise represents an unwanted component that can occur during signal acquisition, transmission, and storage. In this paper, we introduce an efficient method that incorporates redescending M-estimators within the framework of Wiener estimation. The proposed approach effectively suppresses impulsive, additive, and multiplicative noise across varied densities. Our proposed filter operates on both grayscale and color images; it uses local information obtained from the Wiener filter and robust outlier rejection based on Insha and Hampel's tripartite redescending influence functions. The effectiveness of the proposed method is verified through qualitative and quantitative results, using metrics such as PSNR, MAE, and SSIM.

**Keywords:** noise filtering; redescending M-estimator; image processing; multiplicative noise; additive noise; impulsive noise



**Citation:** Rendón-Castro, Á.A.; Mújica-Vargas, D.; Luna-Álvarez, A.; Vianney Kinani, J.M. Enhancing Image Quality via Robust Noise Filtering Using Redescending M-Estimators. *Entropy* **2023**, *25*, 1176. <https://doi.org/10.3390/e25081176>

Academic Editors: Friedhelm Schwenker and Wei Li

Received: 15 May 2023

Revised: 20 July 2023

Accepted: 6 August 2023

Published: 7 August 2023



**Copyright:** © 2023 by the authors. Licensee MDPI, Basel, Switzerland. This article is an open access article distributed under the terms and conditions of the Creative Commons Attribution (CC BY) license (<https://creativecommons.org/licenses/by/4.0/>).

## 1. Introduction

Crucial tasks, such as image processing and medical diagnostics through imaging, require the absence of noise and acceptable quality. This necessitates the suppression of noise without deteriorating fine details or suppressing essential data. Image acquisition, storage, and transmission often introduce various types of noise. For most images, the noise mainly comes from additive, multiplicative, and impulsive noise [1]. Additive noise degrades the image due to pixel intensity fluctuations in the 2D space, with each pixel's degradation characterized by a Gaussian-like distribution (Gaussian noise). Multiplicative noise, also known as speckle noise, is usually generated when images of complex objects are acquired using highly complex waves; it depends on the signal that produces it and it is difficult to eliminate with traditional noise models. Impulsive noise could be modeled by employing fixed intensity pixel values (salt and pepper noise) where some image pixels are altered to 0 or 255 [2–4]. This paper proposes a filter designed to process additive, multiplicative, and impulsive noise using redescending M-estimators. The robust functions implemented are Insha and Hampel's three-part redescending functions, implemented in the context of a Wiener filter due to their advantages in local measures. The proposed work is assessed using PSNR, SSIM, and MAE metrics and compared with four prevalent methods to process the three types of noise.

In this research, our primary motivation for developing this filter using redescending M-estimators stems from the understanding that additive, impulsive, and multiplicative noise are dominant sources of image corruption. Such noise can emerge during image capture and transmission because of uncontrollable environmental factors or sensor-related characteristics. Furthermore, impulsive noise often manifests during image storage and manipulation. Considering these factors collectively, we believe that our proposed application has broad applicability across various fields, with particular significance in the

realm of medical imaging. By mitigating the impact of noise, our solution could assist experts in accurately diagnosing potential pathologies in corrupted images influenced by the aforementioned noise types.

The contribution of this research consists of introducing a noise suppression filter based on redescending M-estimators. The filter is supported by robust processing through the theory of redescending M-estimators, which makes it more tolerant to high noise densities. We compare the proposed filter with four popular filters currently used for general noise suppression. The performance of the filter is evaluated through different experiments, using metrics such as PSNR, SSIM, and MAE.

This paper is organized as follows: In Section 2, we introduce the basic concepts required to understand the work. Section 3 presents the proposed denoising filter and its mathematical background. In Section 4, we present the experimental results and a comparative analysis of the image restoration quality using metrics in comparison to other current methods in the literature. Finally, in Section 5, we provide a synopsis of the main results and recommendations for future work.

## 2. Related Work

Several methods have been developed to address the removal of one or a combination of the three types of noise. For the purposes of this research, these methods can be classified into five major classes [5–7]:

1. Additive and multiplicative filtering: This class includes widely used non-local means (NLM)-based filters [8], which estimate the value of a particular pixel by considering information from the entire image, preserving relevant details. It also includes anisotropic diffusion (AD)-based filters [9,10], which adaptively apply a diffusion process based on the local structure of the image. In [9], an anisotropic diffusion coefficient with an image-dependent threshold parameter was proposed for low densities of Gaussian and speckle noise. While in [10], a method for only suppressing speckle noise was proposed, which combines the use of a Canny operator to enhance an anisotropic diffusion equation. Although these filters are good at preserving details, they fail to handle high noise densities and are not robust against impulse noise. Additionally, bilateral-based filters [11–14] consider both spatial proximity and intensity similarity between pixels, ensuring that nearby pixels have a significant influence on the filtering process. In [11,12], they focus on universal noise suppressors, but they only process Gaussian and impulse noise. Meanwhile, in [13,14], the authors address the optimization and adaptation of the bilateral algorithm to work with color images. This approach, while effective in terms of parameter flexibility and preserving certain edges in images, lacks handling high noise densities, processing multiplicative noise, and certain blurring of details. Another approach involves estimating the noise level by transforming an image into other domains. For example, in [15], a local complexity estimation in the wavelet domain was proposed for MRI denoising. In [16], a collaborative 3D domain transformation was introduced for noise removal. Additionally, in [17], a hidden Markov model was proposed for transforming an image into other spaces and suppressing Gaussian noise. This type of work often leverages the increase/change of information through domain transformation, but image details and noise cannot be completely separated, and certain image characteristics can be lost. One general drawback of the mentioned filters is that they can introduce a certain degree of blurriness in the image. This is due to considering information from the entire image or applying adaptive diffusion processes, which may result in the loss of fine details or the blurring of important edges. This can impact the visual quality and accuracy of the filtered image, especially in areas with sharp intensity or texture changes. Additionally, some of these filters cannot handle high noise densities.

2. Impulsive filtering: This class primarily focuses on nonlinear filters and is commonly addressed through median-based filters, as in [18], where a fuzzy paradigm was also applied. Similarly, iterative mean/median filters were used in the works of Chen [19,20], and robust statistical methods that achieve remarkable results at rejecting atypical data [21],

which is a distinctive characteristic of impulsive noise. These filters typically perform well with high noise densities but are limited to only one type of noise, and their computational costs can be exhaustive due to their iterative processing.

3. Neural networks for noise removal: This category encompasses various approaches. For instance, in [22], a model based on deep convolutional neural networks (CNNs) was proposed for removing multiplicative noise. In [23], a complex-valued CNN was applied for Gaussian denoising. In [24], two deep CNNs were combined to leverage more features for image denoising, and batch renormalization was used to address the small mini-batch problem. Furthermore, in [25], Tian et al. introduced a deep CNN with batch renormalization. Additionally, in [26], the same authors worked with a three-stage CNN by incorporating the wavelet transform, which is highly effective for denoising noisy images corrupted by unknown noise. While these methods can achieve excellent results, they often require substantial resources for designing and training, high computational power, overfitting risks, difficulty in internal interpretation, and sensitivity to the quality and quantity of training data. It is worth noting that these approaches typically rely on extensive training databases, although some methods, like Self2self [27], only use a single image for training. However, their training processes can be very slow.

4. Sparse and low-rank models: These models focus on decomposing a matrix into two components, i.e., a low-rank component and a sparse component. The low-rank component can be approximated as the sum of a relatively small number of column vectors, while the “sparse” component refers to the property of having many zero or near-zero elements. These models are achieved through the minimization of an objective function that penalizes the difference between the original matrix and the sum of the low-rank and sparse matrices. In [28–31], they were applied to hyperspectral images with multiple channels. While these models can work for various types of noise and handle large volumes of data, they also have some limitations. They can be computationally intensive due to the decomposition and reconstruction of the matrices. Additionally, they are sensitive to parameter selection, require appropriate training data, and have limitations in their ability to handle certain types of noise.

5. Robust estimation for filtering: This category involves the application of robust estimation techniques to eliminate impulsive noise. Previous studies have utilized M-estimators. In [32], a median redescending estimator was employed for impulsive denoising in grayscale images. Furthermore, in [33], we extended the median redescending M-estimator for color images, multi-core processing, and random-value impulsive noise. These robust estimations utilize redescending influence functions ( $\psi$ ) for effective impulsive noise elimination. Another approach involves an NLM (non-local means) method for suppressing Gaussian noise using Tukey’s biweight estimation [34].

Therefore, noise suppression represents a challenging task that can be approached from different perspectives. However, the approaches discussed so far often focus on low noise densities and lack the ability to handle all three types of noise. For this reason, in this research, we aim to develop a filter that does not require training and can effectively handle different types of noise, even at high densities. While the primary focus of this research is to contribute to the diversity of approaches in image noise removal methods, we strongly believe in addressing current and future challenges and exploring efficient and adaptable solutions across diverse contexts and applications. Algorithms that go beyond the classes presented in this section offer unique advantages and can serve as valuable complements to enrich the overall research field.

### 3. Principles

#### 3.1. Noise Models

Noise is considered an unwanted component in signal processing, and it can occur during the capturing, processing, and storage of information [35]. If  $f$  is considered a signal, it can be decomposed into a desired component  $g$  and an undesired component representing noise  $q$ . The most common types of noise are additive noise ( $f = g + q$ ),

multiplicative noise ( $f = gq$ ), and impulsive noise ( $f = g(q)$ ). These are the types of noise addressed in this work, and their characteristics are summarized in Table 1.

**Table 1.** Noise models considered in this work [36].

Noise Type	Name	Expression
Additive	Gaussian	$\tilde{x} = \frac{1}{\sigma\sqrt{2\pi}} e^{-\frac{(x-\mu)^2}{2\sigma^2}}$
Multiplicative	Speckle	$\tilde{x} = x + nx$ , $n =$ uniformly distributed random noise
Impulsive	Salt & Pepper	$\tilde{x} = \begin{cases} 0 & \text{with probability } p/2 \text{ (pepper)} \\ x_{i,j} & \text{with probability } p - 1 \\ 255 & \text{with probability } p/2 \text{ (salt)} \end{cases}$

### 3.2. M-Estimators

The maximum likelihood estimator proposed by Huber in 1964 has been generalized to M estimators, offering reasonable bias and flexibility by treating the mean and median as special cases [37]. M estimators, denoted as  $T_n = T_n(x_1, \dots, x_n)$ , minimize the objective function [38–40]:

$$\sum_{i=1}^n \rho(x_i, T_n) \rightarrow \min \quad (1)$$

Here,  $T_n$  represents the desired estimate, and  $\rho$  is the loss function. The minimization problem can also be expressed as follows:

$$\sum_{i=1}^n \psi(x_i, T_n) \quad (2)$$

where  $\psi(x, T_n)$  is the influence function, defined as  $\psi(x, T_n) = \frac{\partial}{\partial T_n} \rho(x, T_n)$ . The loss function  $\rho$  is assumed to be symmetric and positive definite; it has a unique minimum at zero, and possesses a partial derivative.

### 3.3. Redescending M-Estimators

A particular type of M-estimator can completely reject extreme values, which implies that their  $\psi$  functions decay away from the central region and do not decay near the origin. These are called redescending M-estimators and are defined as [41]:

$$\psi_r(x) = \{\psi(x) = 0 \forall |x| \geq r\} \quad (3)$$

where  $0 < r < \infty$  is the threshold that allows the limits of the influence function to be set. Redescending estimators are designed to vanish outside the central region and settle to zero if the threshold  $r$  is reached. Their efficiency is due to function  $\psi$  having a high break point and does not entirely ignore moderately large outliers [42]. The estimators used are Hampel's three-part redescending M-estimator and Insha's redescending M-estimator, which are discussed below.

#### 3.3.1. Hampel's Three-Part Redescending

The Hampel M-estimators maintain a strategic approach to address outliers by delineating regions that mirror the effects of outliers to varying extents. The Hampel three-part redescending estimator is the most suitable for mitigating the influence of outliers. In contrast, other M-estimators, such as Huber's and Tukey's, do not provide the requisite accuracy to ensure an adequate level of precision when confronting specific outlier types. The function of Hampel's three-part redescending estimator, seen as a robust measure, can be interpreted as a combination of the  $l_2$  norm and the  $l_1$  norm, excluding outliers; its function  $\psi$  is given by:

$$\psi_{HAM(a,b,r)}(x_{i,j}) = \begin{cases} x & 0 \leq |x| \leq a \\ a \cdot \text{sgn}(x) & a \leq |x| \leq r \\ a \cdot \frac{r-|x|}{r-b} & b \leq |x| \leq r \\ 0 & 0 \leq |x| \end{cases} \quad (4)$$

The  $\psi$  representation of Hampel’s three-part redescending function is shown in Figure 1.

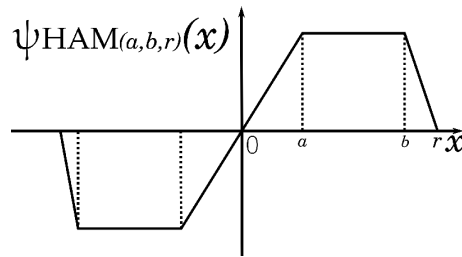


Figure 1. Graph of Hampel’s three-part redescending function.

### 3.3.2. Insha

This estimator covers some drawbacks of the redescending M-estimators and is considered a tool for outlier detection and robust regression [43]. The form and properties of its corresponding  $\psi$  function are discussed below:

$$\rho(x) = \frac{c^2}{4} [\arctan(\frac{x}{c})^2 + \frac{c^2 + x^2}{c^4 + x^4}] \quad \text{for } |x| \geq 0 \quad (5)$$

where  $c$  is the fit constant; for the  $i$ -th observation, variables  $x_i$  are the residuals scaled over MAD. With respect to  $x$ , the following  $\psi$  function is obtained:

$$\psi_{I(r)}(x) = x \cdot [1 + (\frac{x}{c})^4]^2 \quad \text{for } |x| \geq 0. \quad (6)$$

The graph of the  $\psi$  Insha function is shown in Figure 2.

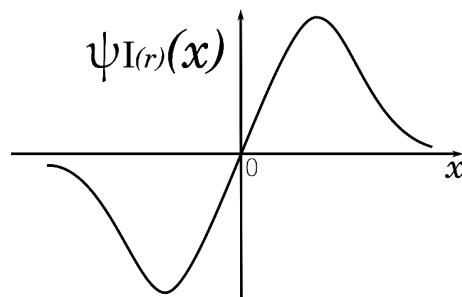


Figure 2. Graph of the Insha function.

## 4. Proposed Noise Suppression Filter

Our proposal focuses on eliminating additive and multiplicative noise with the Insha estimator because the normal distribution of these noises can be optimally modeled through this approach. For impulsive noise, Hampel’s three-part estimator is used, which has an adaptive behavior by the MAD component that allows, through its thresholds, the correct suppression of impulsive noise. To make the process more robust, we follow the structure of the Wiener filter. Wiener filtering minimizes the overall mean square error in the inverse filtering and noise smoothing process. Wiener estimates the local mean and variance around each pixel [44].

$$\mu = \frac{1}{NM} \sum_{n_1, n_2 \in \eta} a(n_1, n_2), \quad (7)$$

and

$$\sigma^2 = \frac{1}{NM} \sum_{n_1, n_2 \in \eta} a^2(n_1, n_2) - \mu^2, \tag{8}$$

where  $\eta$  is the local  $N \times M$  neighborhood of each pixel in image  $X$ . Wiener creates a per-pixel Wiener filter using these estimates. Using the above measurements, we have the following equation:

$$b(n_1, n_2) = \mu + \frac{\sigma^2}{v^2} (a(n_1, n_2) - \mu). \tag{9}$$

where  $v^2$  is the variance of the noise. If the noise variance is not given, Wiener uses the average of all estimated local variances. Then, considering the above, we rewrite the local means in terms of a redescending estimator:

$$\mu(\hat{x}) = \frac{1}{nm} \sum_{i,j} \psi(x) \tag{10}$$

where  $\tilde{x}$  is the observation of the noisy image and  $\hat{x}$  is the result of the component of the Wiener filter. The local variance is as follows:

$$\zeta^2(\hat{x}) = \frac{1}{nm} \sum_{i,j \in \eta} \psi^2(x_{ij}) - \mu^2(x) \tag{11}$$

The noise variance is as follows:

$$v^2(\hat{x}) = k \cdot \text{med}\{|\psi x_{ij} - \text{med}(\psi(x_\eta))|\} \tag{12}$$

where  $k$  is a scaling factor for normally distributed data; it uses the reciprocal of the quantile function  $\Phi^{-1}$ , while  $3/4$  represents the portion that covers 50% (between  $1/4$  and  $3/4$ ) of the standard normal cumulative distribution function:

$$k = \frac{1}{\Phi^{-1} \frac{3}{4}} = 1.4826 \tag{13}$$

As a result of the above equations, using a filter with the Wiener structure but operating with the properties of the redescending M-estimator, we have the following:

$$\tilde{x} = \psi(x) + \frac{\zeta^2(\hat{x}) - v^2(\hat{x})}{\zeta^2(\hat{x})} \cdot (x - \psi(x)) \tag{14}$$

The influence function  $\psi$  can take the value of Insha =  $\psi_{I(r)}$  or Hampel =  $\psi_{HAM(a,b,r)}$ , depending on the noise to be processed. Thus, we combine the two non-parametric methods that allow the elimination of impulsive and multiplicative noise by utilizing a Wiener smoothing procedure and the robustness provided by a redescending M-estimator. The influence functions used are shown in Table 2.

**Table 2.** Modified influence functions of the redescending M-estimator.

Influence Function	Formulae	Thresholds
Insha	$\psi_{I(r)}(x) = x \cdot [1 + (\frac{x}{c})^4]^2$ for $ x  \geq 0$	$c = k \cdot \text{Med}( \tilde{x}_i - \text{Med}(h) )$
Hampel's three-part redescending	$\psi_{HAM(a,b,r)}(x) = \begin{cases} x & 0 \leq  x  \leq a \\ a \cdot \text{sgn}(x) & a \leq  x  \leq r \\ a \cdot \frac{r- x }{r-b} & b \leq  x  \leq r \\ 0 & 0 \leq  x  \end{cases}$	$r = k \cdot \text{Med}( \tilde{x}_i - \text{Med}(h) )$ , $a = 0.15 \cdot r$ and $b = 0.85 \cdot r$

### Proposed Algorithm

The basic structure of the filtering process can be seen in the pseudocode Algorithm 1.

---

#### Algorithm 1 Robust redescending M-estimator filter.

---

**Require:** Noisy image  $X$  in grayscale with size  $N \times M$ .

**Ensure:** Select an influence function of Table 2, depending on the type of noise.

- 1: **for**  $i = 1$  to  $M$  **do**
- 2:     **for**  $j = 1$  to  $N$  **do**
- 3:          $\mu(\hat{x}) \leftarrow \frac{1}{nm} \sum_{i,j} \psi(x)$  ▷ Compute local mean.
- 4:          $\sigma^2(\hat{x}) \leftarrow \frac{1}{nm} \sum_{i,j \in \eta} \psi(x^2 - \mu^2(x))$  ▷ Compute local variance.
- 5:          $v^2(\hat{x}) = 1.4823 \cdot \text{med}\{|\psi x - \text{med}(\psi(x))|\}$  ▷ Compute noise variance.
- 6:          $\tilde{x} = \psi(x) + \frac{\sigma^2(\hat{x}) - v^2(\hat{x})}{\sigma^2(\hat{x})} \cdot (x - \psi(x))$  ▷ Redescending M-estimator.
- 7:          $Y_{i,j} \leftarrow \tilde{x}$  ▷ The calculated value is written in the output image.
- 8:     **end for**
- 9: **end for**

**Output:** Filtered image  $Y$  with size  $M \times N$ .

---

## 5. Experimentation and Results

The performance of the proposed filter is validated through three tests: standard and medical grayscale image processing, image size and batch processing, color image and video processing.

### 5.1. Standard and Medical Grayscale Image Processing

In the first instance, this experiment was carried out using quality metrics and test images, such as the standard Lena ( $512 \times 512$  size), lbox\_66720-Afbeelding7 ( $437 \times 520$  size and abbreviated as e2), mdb332DNORM ( $425 \times 390$  size and abbreviated as e3), and 00000152\_016 ( $272 \times 530$  size and abbreviated as e4) from the datasets [45–47]. In the execution, images were corrupted by additive and multiplicative noise from 0.02 to 0.12 in variance, and impulsive from 0.1 to 0.6. The performance of our filter was compared with four state-of-the-art filtering methods that were highly tested to suppress different kinds of noise, such as non-local means (NLM) [48,49], BM3D [16], bilateral filter [14], trilateral filter [11], and estimate parameters for anisotropic diffusion filtering [50,51]. We programmed the proposed filter in MATLAB via an Intel(R) Core(TM) processor i5-8400 CPU @2.8 GHz with six cores and 32 GB of RAM. The comparative methods for ease were also implemented in MATLAB. The metrics used were the following.

The noise suppressing quality was quantified by using the peak signal-to-noise ratio (PSNR) [52] and structural similarity index (SSIM) [53]; the mean absolute error (MAE) was used to quantify the preservation of the fine details of the image [52]. These three metrics can be determined from the following expressions:

$$\text{PSNR} = 10 \cdot \log \left[ \frac{(\max(x(i,j)))^2}{\text{MSE}} \right], \quad (15)$$

where MSE is the mean squared error and is determined by:

$$\text{MSE} = \frac{1}{M \cdot N} \sum_{i=1}^M \sum_{j=1}^N [x(i,j) - \hat{e}(i,j)]^2, \quad (16)$$

where  $M \cdot N$  represents the image sizes that are analyzed,  $x(i,j)$  is the original image, and  $\hat{e}(i,j)$  is the improved image. The SSIM metric, in a simplified form, is calculated by the following expression:

$$SSIM(x,y) = \frac{(2\mu_x\mu_y + C_1) \cdot (2\sigma_{xy} + C_2)}{(\mu_x^2\mu_y^2 + C_1) \cdot (\sigma_x^2 + \sigma_y^2 + C_2)}, \tag{17}$$

where  $x$  is the original image,  $y$  is the refined image,  $\mu_x$  and  $\mu_y$  are the luminance values,  $\sigma_x$  and  $\sigma_y$  are the contrast values, and  $C_1$  and  $C_2$  are two constant values. On the other hand, MAE can be computed by:

$$MAE = \frac{1}{M \cdot N} \sum_{i=1}^M \sum_{j=1}^N [x(i, j) - \hat{e}(i, j)], \tag{18}$$

The results of experimentation with the PSNR, SSIM, and MAE metrics can be observed in Table 3 for the Lena grayscale image. According to the table, we can see that the proposed filter—considering the redescending influence functions at the lowest densities—has a lower-medium performance. However, as the noise density increases, the performance of our proposed filter is more efficient than the comparative filters, above all, for multiplicative noise.

**Table 3.** Restoration results in PSNR, SSIM, and MAE terms for Lena for the proposed method. Additive (A), multiplicative (M), impulsive (I), bilateral (Bi), and trilateral (Tri).

Noise Type	Noise Density	Denoising Method																	
		PSNR						SSIM						MAE					
		R	NLM	AD	BM3D	Bi	Tri	R	NLM	AD	BM3D	Bi	Tri	R	NLM	AD	BM3D	Bi	Tri
A	0.02	27.71	28.30	26.69	17.061	18.274	30.45	0.74	0.75	0.65	0.45	0.36	0.74	0.0227	0.0223	0.0208	0.0675	0.0980	0.0323
	0.04	26.37	26.34	24.18	15.088	15.622	29.542	0.67	0.66	0.54	0.44	0.32	0.66	0.0361	0.0348	0.0387	0.0936	0.1340	0.0505
	0.06	25.33	25.08	23.09	13.921	14.186	25.257	0.62	0.60	0.54	0.44	0.30	0.62	0.0415	0.0412	0.0468	0.1136	0.1593	0.0597
	0.08	24.48	24.16	22.28	13.123	13.250	24.514	0.59	0.56	0.50	0.43	0.30	0.57	0.0467	0.0470	0.0486	0.1298	0.1787	0.0682
	0.1	23.72	23.38	21.44	12.517	12.580	23.700	0.56	0.53	0.45	0.43	0.29	0.54	0.0511	0.0511	0.0514	0.1436	0.1944	0.0741
	0.12	22.99	22.77	21.00	12.030	12.072	23.011	0.53	0.50	0.51	0.42	0.29	0.48	0.0554	0.0563	0.0543	0.1559	0.2074	0.0816
M	0.02	29.01	30.24	30.46	18.433	23.460	23.425	0.81	0.79	0.82	0.38	0.51	0.79	0.0227	0.0223	0.0208	0.0538	0.0538	0.0323
	0.04	28.46	28.47	28.43	16.525	20.758	21.752	0.78	0.72	0.77	0.36	0.45	0.67	0.0254	0.0270	0.0279	0.0741	0.0737	0.0392
	0.06	27.95	27.59	27.31	15.397	19.167	20.276	0.75	0.68	0.72	0.35	0.41	0.64	0.0279	0.0303	0.0303	0.0893	0.0887	0.0439
	0.08	27.46	26.72	26.43	14.569	18.033	20.045	0.73	0.65	0.70	0.34	0.39	0.61	0.0301	0.0334	0.0324	0.1026	0.1015	0.0484
	0.1	27.04	26.06	25.72	13.936	17.161	19.873	0.71	0.62	0.69	0.34	0.37	0.58	0.0321	0.0357	0.0353	0.1139	0.1123	0.0518
	0.12	26.67	25.59	25.12	13.409	16.442	19.742	0.70	0.60	0.66	0.33	0.36	0.75	0.0339	0.0382	0.0363	0.1244	0.1221	0.0554
I	0.1	26.08	21.73	14.78	13.647	16.635	30.436	0.53	0.40	0.12	0.36	0.36	0.55	0.0347	0.0317	0.0572	0.0949	0.0733	0.0460
	0.2	21.96	22.65	13.74	11.503	13.713	28.456	0.50	0.37	0.24	0.35	0.31	0.54	0.0502	0.0471	0.0662	0.1509	0.1254	0.0683
	0.3	19.06	20.20	13.20	10.343	12.052	21.450	0.47	0.32	0.35	0.35	0.29	0.54	0.0658	0.0633	0.0766	0.1942	0.1718	0.0918
	0.4	16.77	17.75	12.33	9.474	10.835	18.562	0.45	0.29	0.37	0.35	0.28	0.49	0.0834	0.0782	0.0858	0.2327	0.2165	0.1134
	0.5	15.01	15.83	11.73	8.825	9.943	14.943	0.39	0.26	0.38	0.35	0.27	0.45	0.1015	0.0916	0.0929	0.2659	0.2566	0.1328
	0.6	13.47	14.17	12.10	8.306	9.202	14.202	0.35	0.24	0.36	0.34	0.27	0.35	0.1225	0.1055	0.1040	0.2954	0.2946	0.1530

The results can be more easily identified in the graphs of Figure 3. These graphs show the average of the metrics for the four test images using the Insha estimator for additive and multiplicative noise, exhibiting a more tolerant behavior with increasing noise density. On the other hand, for the Hampel estimator, an inverse behavior is observed, as it has a more efficient performance at low densities of impulsive noise. However, as the noise density increases, it becomes more affected.

Figure 4 confirms that the filtered Lena image using redescending functions aligns with the expected metric results. Improved performance is observed at high noise densities for both additive and multiplicative noise with the Insha estimator, while visually, the processed images exhibit better preservation of details. In contrast, the Hampel estimator shows superior results for impulsive noise at low densities.



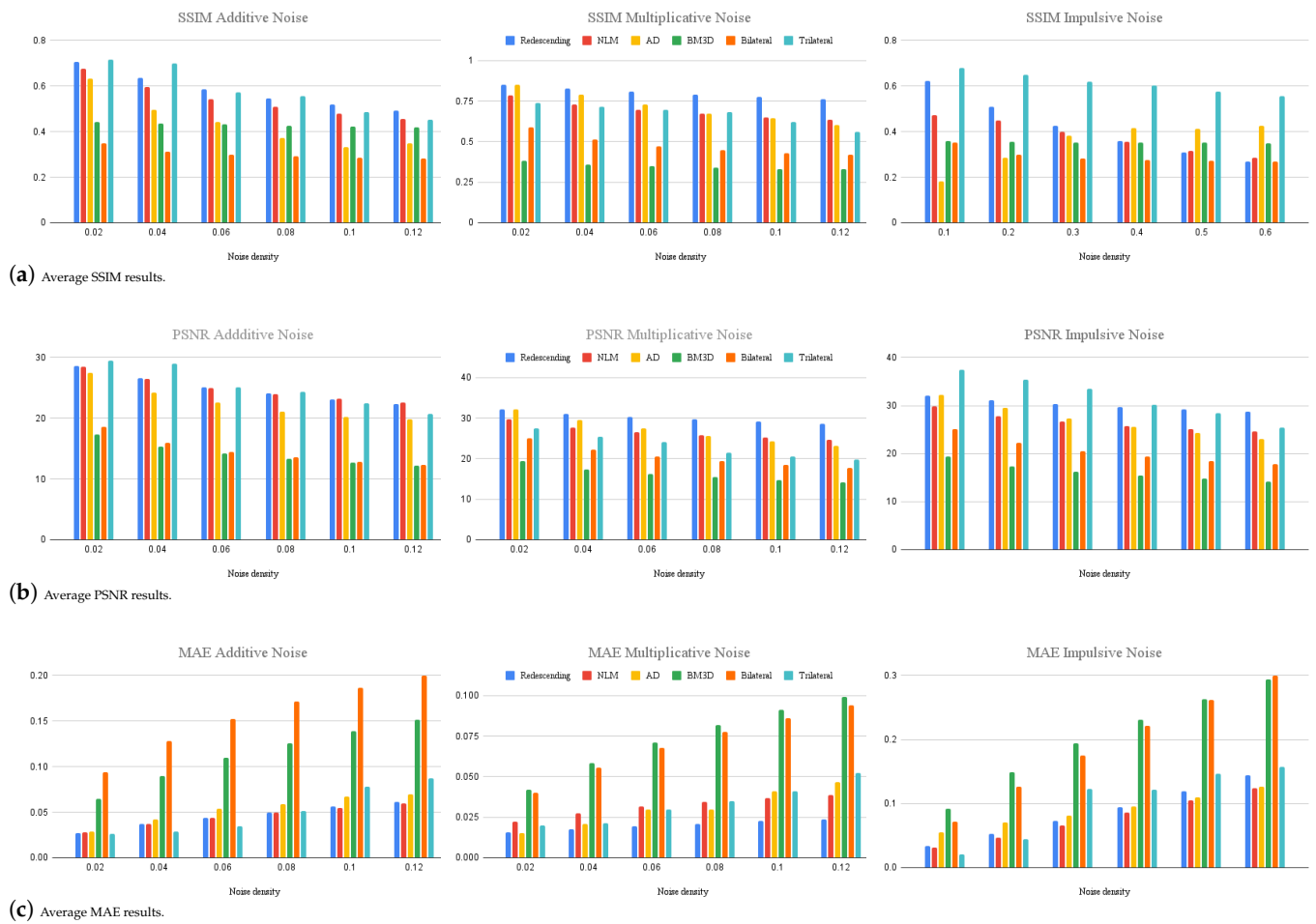


Figure 3. Graphical illustrations of the average results of the metrics for the four test images.

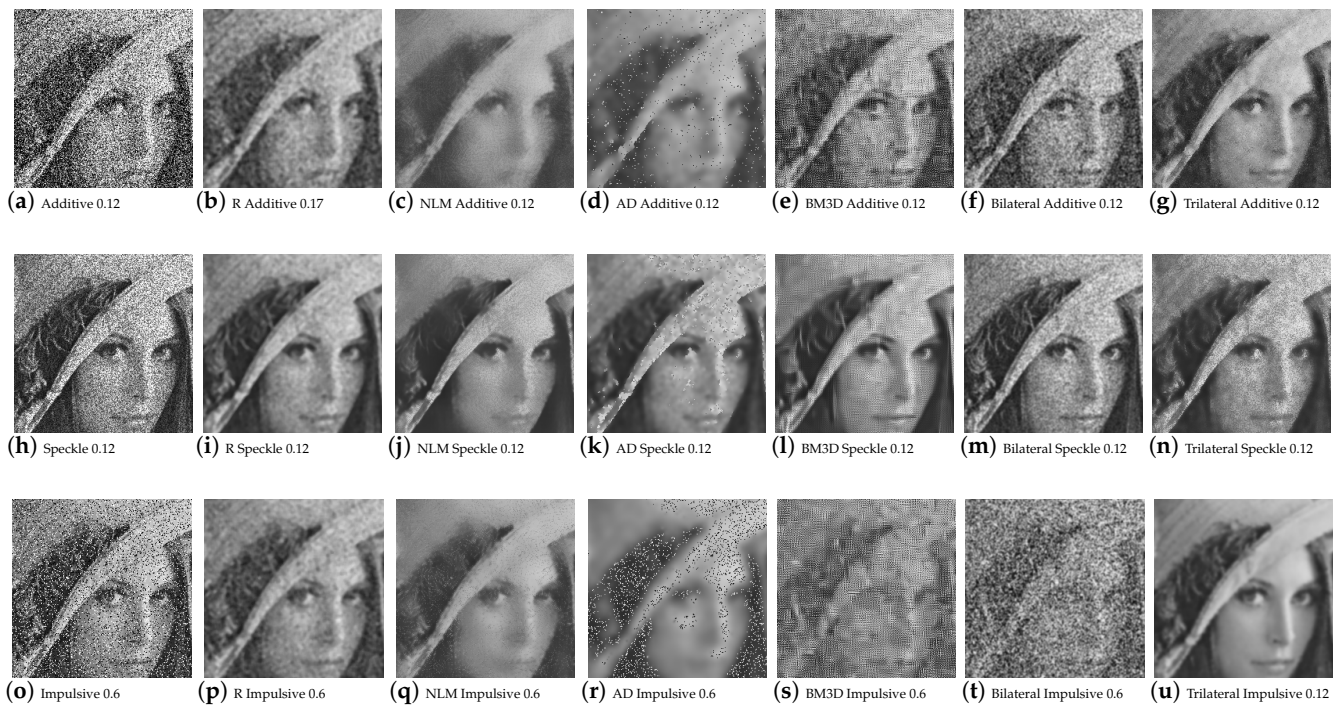
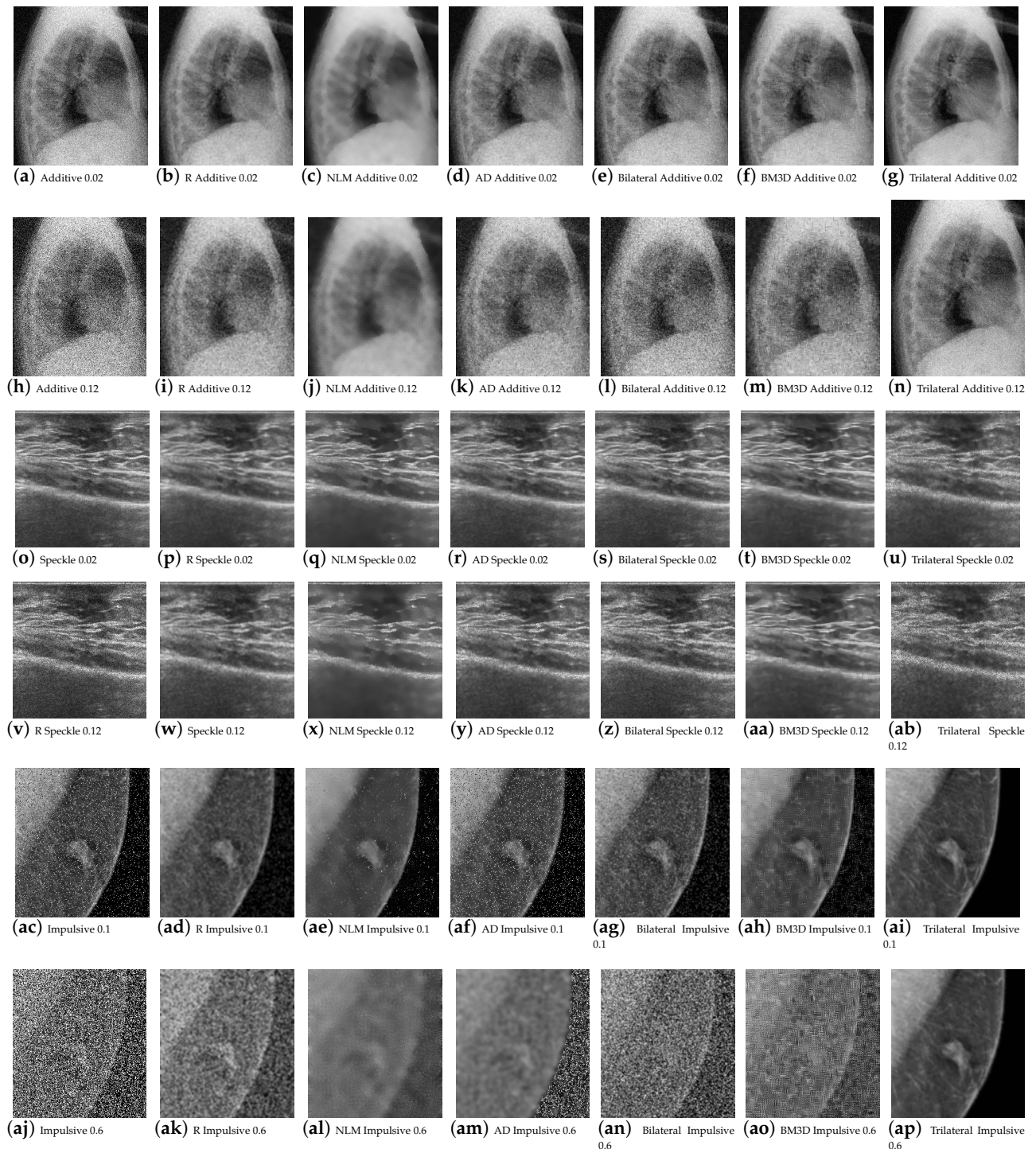


Figure 4. Qualitative results of the redescending (R), NLM, AD, BM3D, and bilateral Lena image.

Figure 5 presents the results for images e2, e3, and e4, demonstrating the effectiveness of the proposed filter in efficiently removing various types of noise from medical images.



**Figure 5.** Results of redescending (R), NLM, and AD for the existing and proposed methods at low noise densities (additive = 0.02, multiplicative = 0.02, and impulsive = 0.1) and high noise densities (additive = 0.12, multiplicative = 0.12, and impulsive = 0.6).

### 5.2. Image Size and Batch Processing

To assess the algorithm's complexity, the execution times of various algorithms were measured using the resized grayscale Lena image. The results of this experiment are shown in Table 4. The results indicate that the proposed approach has a reasonable execution time

compared to the comparative methods. However, it is worth noting that utilizing a GPU is recommended to further accelerate the execution time of the proposed method.

**Table 4.** Average execution times (in seconds) with the increasing image size in the Lena image; bold indicates the fastest and underlined denotes the slowest.

Algorithm/Size	281.7 kB 768 × 768	436.1 kB 1024 × 1024	607.9 kB 1280 × 1024	783.9 kB 1536 × 1024
Redescending	13.76	25.59	37.68	54.52
NLM	5.06	54.71	119.82	139.78
AD	20.36	45.83	60.68	91.43
BM3D	<u>25.66</u>	46.88	66.82	96.16
Bilateral	<b>0.09</b>	<b>0.143</b>	<b>0.22</b>	<b>0.31</b>
Trilateral	10.4	21.56	55.76	82.45

In general, it can be said that the proposed algorithm has a complexity of  $O(n^2)$  since it iterates through all the pixels of the image, and for each pixel, a specific calculation is performed depending on the type of noise. However, for the multiplicative and impulsive noise types, better results are usually obtained compared to the compared algorithms.

To validate the effectiveness of our proposed approach, it was implemented on various datasets to assess its performance across different densities of the three types of noise. The datasets used included the mammographic image analysis society digital mammogram database (MIAS) [46], comprising one hundred images, twelve standard grayscale images from BSD68 [54], and fifty images from the dataset of breast ultrasound images (DBUI) [55]. The results obtained for different noise densities demonstrated satisfactory performance across different image types. The results of the highest densities of each noise type are presented in Table 5.

**Table 5.** Results of the different datasets with additive noise = 0.12, multiplicative noise = 0.12, and impulsive noise = 0.6 .

Dataset	Noise	Algorithm	PSNR	SSIM	MAE	Dataset	PSNR	SSIM	MAE	Dataset	PSNR	SSIM	MAE
MIAS	Additive	Redescending	18.43	0.57	0.0244	BSD68	21.37	0.88	0.017	DBUI	21.60	0.63	0.017
		NLM	18.65	0.58	0.0242		21.52	0.88	0.017		21.71	0.61	0.017
		AD	17.61	0.55	0.0251		18.47	0.78	0.019		18.74	0.43	0.020
		BM3D	13.33	0.38	0.0431		13.74	0.50	0.041		13.57	0.13	0.042
		Bilateral	18.23	0.60	0.0257		19.75	0.82	0.021		19.90	0.47	0.021
		Trilateral	18.11	0.51	0.020		18.01	0.77	0.016		22.07	0.59	0.017
	Multiplicative	Redescending	20.65	0.64	0.019	25.80	0.95	0.009	25.91	0.77	0.009		
		NLM	20.59	0.71	0.018	23.96	0.92	0.011	23.07	0.68	0.012		
		AD	20.14	0.68	0.018	22.17	0.89	0.012	22.11	0.69	0.012		
		BM3D	18.70	0.57	0.021	19.64	0.82	0.018	20.77	0.57	0.016		
		Bilateral	21.11	0.54	0.016	24.84	0.93	0.011	25.36	0.75	0.010		
		Trilateral	22.98	0.63	0.018	21.45	0.79	0.022	22.7	0.65	0.014		
	Impulsive	Redescending	16.41	0.51	0.026	18.70	0.80	0.016	15.76	0.33	0.035		
		NLM	14.71	0.34	0.040	15.13	0.58	0.038	13.87	0.30	0.036		
		AD	13.63	0.29	0.041	11.39	0.29	0.045	14.18	0.17	0.040		
		BM3D	10.54	0.17	0.058	10.69	0.24	0.057	10.74	0.05	0.057		
		Bilateral	13.66	0.30	0.043	13.89	0.43	0.042	18.81	0.45	0.017		
		Trilateral	13.97	0.30	0.027	16.40	0.55	0.041	22.54	0.46	0.014		

### 5.3. Color Image and Video Processing

The necessary adjustments were made to implement the filtering algorithms for color images, specifically for images in the RGB color space (red, green, and blue). These adjustments focused on separating the images into their three RGB channels, processing each channel separately, and then recombining the images at the end. From each image, three copies were created with impulsive, additive, and multiplicative noise, respectively. The impulsive noise copies were processed using the Hampel estimator, while the images with additive and multiplicative noise were processed using the Insha estimator. In addition to the proposed filtering algorithms, non-local means (NLM), anisotropic diffusion (AD), bilateral, block-matching, and 3D filtering (BM3D) algorithms were also implemented in the images. Thus, 108 resulting images were obtained from each image.

The fact that three channels of information are now being processed has resulted in an increase in information, which in turn has led to improved performance for the proposed work. For high-density noise experimentation, the standard color images, i.e., Lena, Baboon, Goldhill, Boats, Barbara, and Peppers, were used, along with a positron emission tomography (PET) image. Quantitative results for color image filtering can be seen in Figure 6 for the baboon image and in Figure 7 for brain PET. One can observe how the increase in information benefits the proposed filter, especially for impulsive noise.

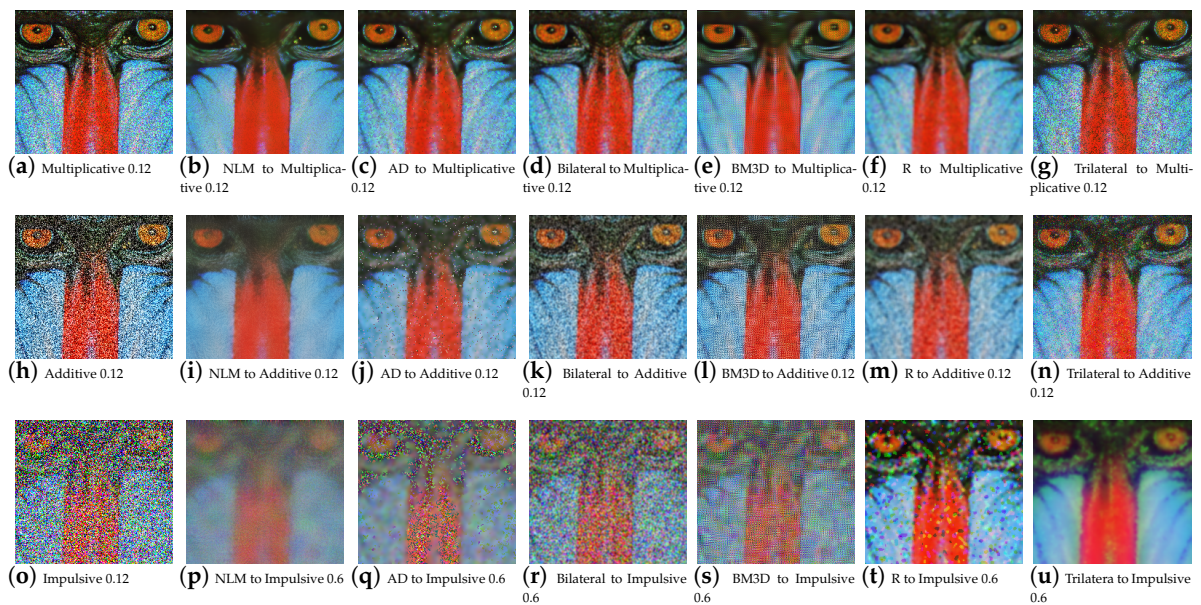


Figure 6. Qualitative results of the redescending (R), NLM, AD, BM3D, and bilateral for the baboon color image.

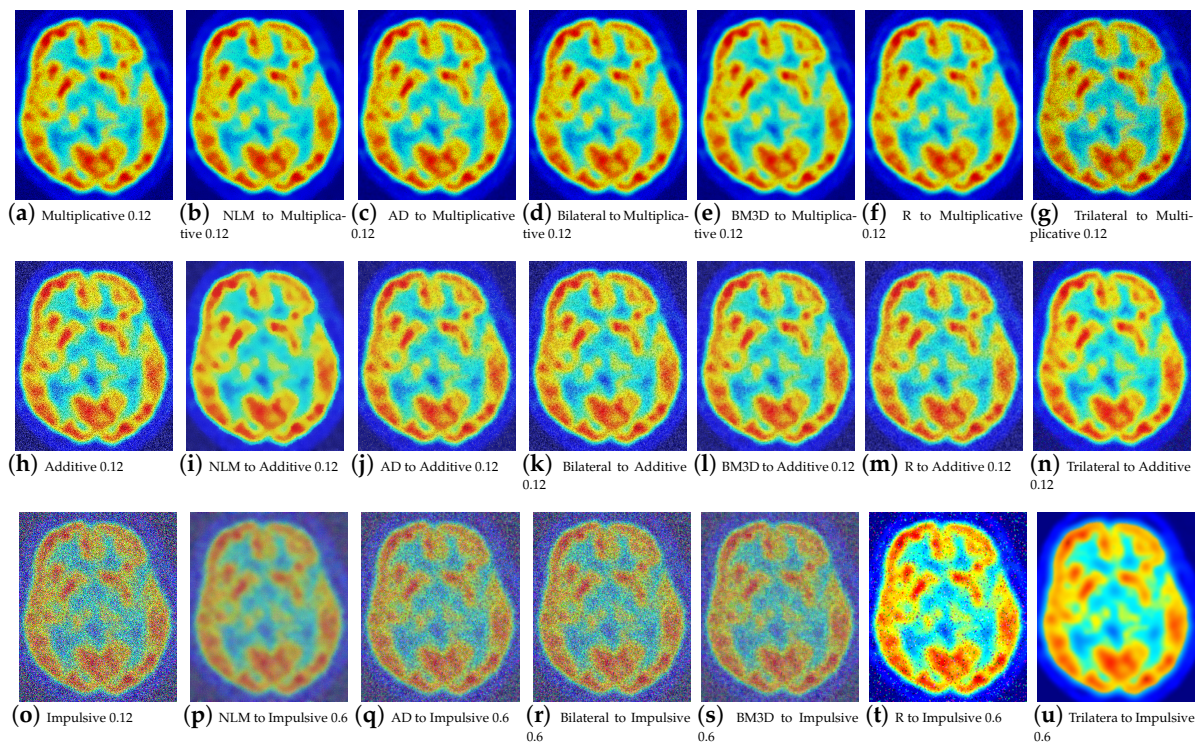
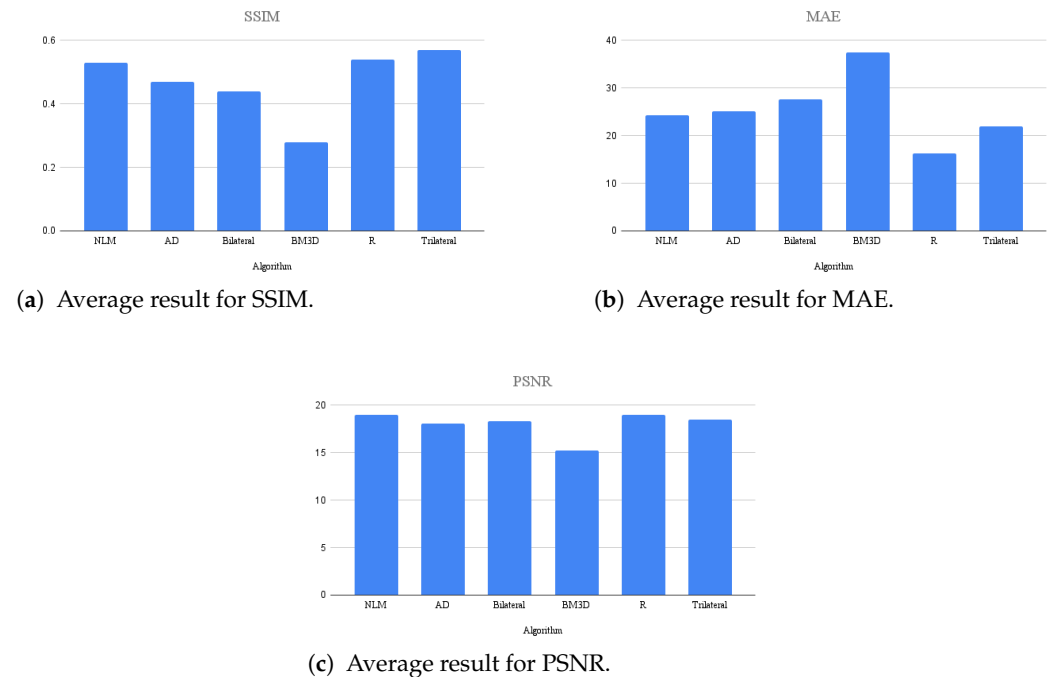


Figure 7. Results of filtering of the brain PET image at high densities.

An experiment was conducted with algorithms using the color image datasets Kodak24 [56] and CBSD68 [54] at the highest levels of density used in this work. The average results of the three types of noise can be observed in the graphs of Figure 8, where the proposed filter performs better in the SSIM and MAE metrics, and second best in the PSNR metric.



**Figure 8.** Average results for high noise densities in color datasets Kodak24 and CBSD68.

Another additional objective involved processing large batches of images, particularly in videos. For this implementation, a corrupted ultrasound video was used. The formulated NLM and Wiener estimators and algorithms were implemented. The video consists of 687 frames, each with dimensions of 540x360 pixels. Some of these frames can be seen in Figure 9.

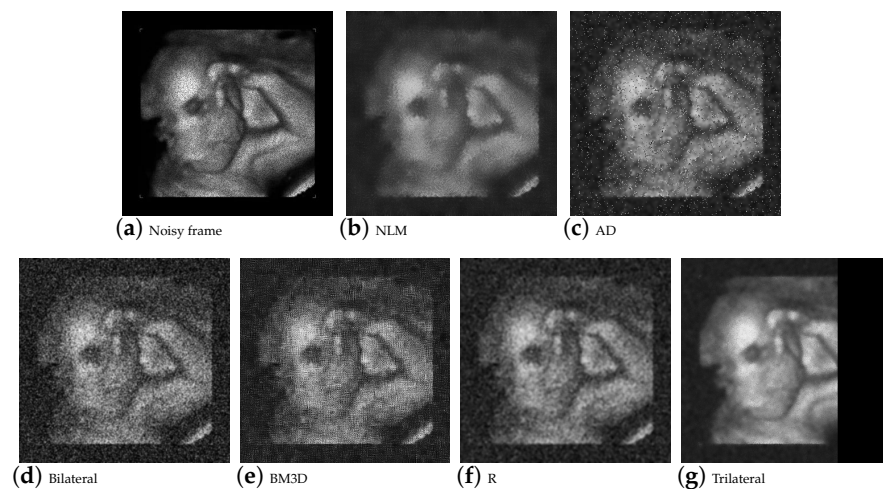


**Figure 9.** Results of the filtering of a frame from the video ultrasound.

To evaluate this implementation, a no-reference image quality metric called the naturalness image quality evaluator (NIQE) was used. NIQE operates exclusively by measuring quantifiable deviations from statistical patterns observed in natural images, without relying on any prior knowledge or information.

In Figure 10, the proposed filter achieved a lower value compared to the others in the proposed work. Having a low value means that the image quality is perceived as good. The NIQE metric is used to evaluate the visual quality of images and provides a numerical score, indicating how close an image is to being perceived as natural by humans. Therefore, a low value in the NIQE metric indicates that the image has good visual quality.

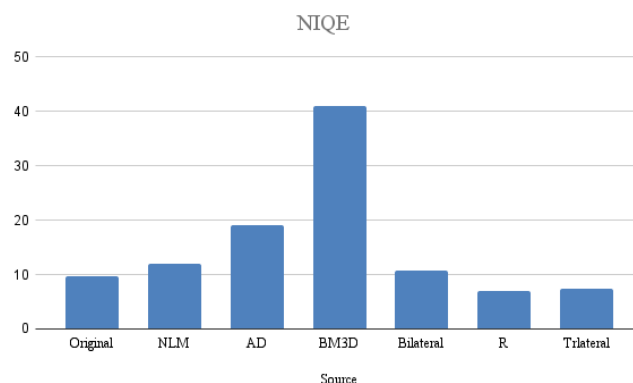


Figure 10. Graphical illustrations of the NIQE metrics.

## 6. Conclusions

This work proposes a robust filter for noise suppression based on redescending M-estimators. The aim is to provide a filter that could restore images from additive, multiplicative and impulsive noise. An application in the medical image field could help experts diagnose possible pathologies better. We propose using two influence functions. The first is the Insha; due to its approximation to a normal distribution, it allows the elimination of additive and multiplicative noise. The second, Hampel's three-part redescending, was used to suppress impulsive noise. The proposed filter shows better performances compared to MLN and AD filters in terms of PSNR, SSIM, and MAE for high additive and multiplicative noise densities, while for the impulsive noise, the best results were at low densities. Considering the processing of RGB images, positive results were obtained according to the metrics, partly due to the information gain resulting from the three channels. Additionally, in the video processing experiment, a good result was indicated through the NIQE metric. In future work, we will consider that the functions can be improved through iterative processes, implementing a noise detector, and incorporating additional or different robust functions. However, it is important to note that this may come with high computational costs, so we could also focus on exploring parallel processing.

**Author Contributions:** Formal analysis, Á.A.R.-C., D.M.-V., A.L.-Á. and J.M.V.K.; investigation, Á.A.R.-C., D.M.-V. and A.L.-Á.; methodology, Á.A.R.-C., D.M.-V. and J.M.V.K.; software, Á.A.R.-C., A.L.-Á.; supervision, D.M.-V.; validation, Á.A.R.-C., D.M.-V. and J.M.V.K.; writing—original draft, Á.A.R.-C., D.M.-V. and A.L.-Á.; writing—review and editing, Á.A.R.-C., D.M.-V. and A.L.-Á. All authors have read and agreed to the published version of the manuscript.

**Funding:** This research received no external funding.

**Institutional Review Board Statement:** Not applicable.

**Informed Consent Statement:** Not applicable.

**Data Availability Statement:** Not applicable.

**Acknowledgments:** The authors thank CONACYT and TecNM-CENIDET for their financial support through the project "Delimitación de masas sólidas malignas en mamografías mediante un algoritmo de nodos conectados con el menor ángulo polar".

**Conflicts of Interest:** The authors declare no conflicts of interest.

## References

1. Distante, A.; Distante, C. *Handbook of Image Processing and Computer Vision*; Springer: Cham, Switzerland, 2020.
2. Distante, A.; Distante, C. *Handbook of Image Processing and Computer Vision: Volume 2: From Image to Pattern*; Springer: Cham, Switzerland, 2020.
3. Bovik, A.C. *The Essential Guide to Image Processing*; Academic Press: Cambridge, MA, USA, 2009.
4. Astola, J.; Kuosmanen, P. *Fundamentals of Nonlinear Digital Filtering*; CRC Press: Boca Raton, FL, USA, 2020.
5. Afshari, H.H.; Gadsden, S.A.; Habibi, S. Gaussian filters for parameter and state estimation: A general review of theory and recent trends. *Signal Process.* **2017**, *135*, 218–238. [[CrossRef](#)]
6. George, G.; Oommen, R.M.; Shelly, S.; Philipose, S.S.; Varghese, A.M. A survey on various median filtering techniques for removal of impulse noise from digital image. In Proceedings of the 2018 Conference on Emerging Devices and Smart Systems (ICEDSS), Tiruchengode, India, 2–3 March 2018; pp. 235–238.
7. Jaybhay, J.; Shastri, R. A study of speckle noise reduction filters. *Signal Image Process. Int. J.* **2015**, *6*, 71–80. [[CrossRef](#)]
8. Singh, K.; Ranade, S.K.; Singh, C. Comparative performance analysis of various wavelet and nonlocal means based approaches for image denoising. *Optik* **2017**, *131*, 423–437. [[CrossRef](#)]
9. Gupta, B.; Lamba, S.S. An efficient anisotropic diffusion model for image denoising with edge preservation. *Comput. Math. Appl.* **2021**, *93*, 106–119.
10. Zhan, X.; Gan, C.; Ding, Y.; Hu, Y.; Xu, B.; Deng, D.; Liao, S.; Xi, J. Speckle Noise Suppression Based on Empirical Mode Decomposition and Improved Anisotropic Diffusion Equation. *Photonics* **2022**, *9*, 611. [[CrossRef](#)]
11. Garnett, R.; Huegerich, T.; Chui, C.; He, W. A universal noise removal algorithm with an impulse detector. *IEEE Trans. Image Process.* **2005**, *14*, 1747–1754. [[CrossRef](#)]
12. Lin, C.H.; Tsai, J.S.; Chiu, C.T. Switching bilateral filter with a texture/noise detector for universal noise removal. *IEEE Trans. Image Process.* **2010**, *19*, 2307–2320.
13. Banterle, F.; Corsini, M.; Cignoni, P.; Scopigno, R. A low-memory, straightforward and fast bilateral filter through subsampling in spatial domain. In *Computer Graphics Forum*; Blackwell Publishing Ltd.: Oxford, UK, 2012; Volume 31, pp. 19–32.
14. Tomasi, C.; Manduchi, R. Bilateral filtering for gray and color images. In Proceedings of the Sixth International Conference on Computer Vision (IEEE Cat. No. 98CH36271), Bombay, India, 7 January 1998; pp. 839–846.
15. Orea-Flores, I.Y.; Gallegos-Funes, F.J.; Arellano-Reynoso, A. Local complexity estimation based filtering method in wavelet domain for magnetic resonance imaging denoising. *Entropy* **2019**, *21*, 401. [[CrossRef](#)]
16. Dabov, K.; Foi, A.; Katkovnik, V.; Egiazarian, K. Image denoising by sparse 3-D transform-domain collaborative filtering. *IEEE Trans. Image Process.* **2007**, *16*, 2080–2095. [[CrossRef](#)]
17. Khmag, A.; Al Haddad, S.A.R.; Ramlee, R.A.; Kamarudin, N.; Malallah, F.L. Natural image noise removal using nonlocal means and hidden Markov models in transform domain. *Vis. Comput.* **2018**, *34*, 1661–1675. [[CrossRef](#)]
18. Toh, K.K.V.; Isa, N.A.M. Noise adaptive fuzzy switching median filter for salt-and-pepper noise reduction. *IEEE Signal Process. Lett.* **2009**, *17*, 281–284. [[CrossRef](#)]
19. Chen, J.; Zhan, Y.; Cao, H.; Xiong, G. Iterative grouping median filter for removal of fixed value impulse noise. *IET Image Process.* **2019**, *13*, 946–953. [[CrossRef](#)]
20. Chen, F.; Huang, M.; Ma, Z.; Li, Y.; Huang, Q. An iterative weighted-mean filter for removal of high-density salt-and-pepper noise. *Symmetry* **2020**, *12*, 1990. [[CrossRef](#)]
21. Shevlyakov, G. Highly Efficient Robust and Stable M-Estimates of Location. *Mathematics* **2021**, *9*, 105. [[CrossRef](#)]
22. Wang, G.; Pan, Z.; Zhang, Z. Deep CNN Denoiser prior for multiplicative noise removal. *Multimed. Tools Appl.* **2019**, *78*, 29007–29019. [[CrossRef](#)]
23. Quan, Y.; Chen, Y.; Shao, Y.; Teng, H.; Xu, Y.; Ji, H. Image denoising using complex-valued deep CNN. *Pattern Recognit.* **2021**, *111*, 107639. [[CrossRef](#)]
24. Chang, Y.; Yan, L.; Chen, M.; Fang, H.; Zhong, S. Two-stage convolutional neural network for medical noise removal via image decomposition. *IEEE Trans. Instrum. Meas.* **2019**, *69*, 2707–2721. [[CrossRef](#)]
25. Tian, C.; Xu, Y.; Zuo, W. Image denoising using deep CNN with batch renormalization. *Neural Netw.* **2020**, *121*, 461–473. [[CrossRef](#)]
26. Tian, C.; Zheng, M.; Zuo, W.; Zhang, B.; Zhang, Y.; Zhang, D. Multi-stage image denoising with the wavelet transform. *Pattern Recognit.* **2023**, *134*, 109050. [[CrossRef](#)]
27. Quan, Y.; Chen, M.; Pang, T.; Ji, H. Self2self with dropout: Learning self-supervised denoising from single image. In Proceedings of the IEEE/CVF Conference on Computer Vision and Pattern Recognition, Seattle, WA, USA, 13–19 June 2020; pp. 1890–1898.
28. Wan, Y.; Ma, A.; He, W.; Zhong, Y. Accurate multi-objective low-rank and sparse model for hyperspectral image denoising method. *IEEE Trans. Evol. Comput.* **2023**, *27*, 37–51. [[CrossRef](#)]
29. Zhang, H.; Liu, L.; He, W.; Zhang, L. Hyperspectral image denoising with total variation regularization and nonlocal low-rank tensor decomposition. *IEEE Trans. Geosci. Remote. Sens.* **2019**, *58*, 3071–3084. [[CrossRef](#)]
30. Xie, T.; Li, S.; Sun, B. Hyperspectral images denoising via nonconvex regularized low-rank and sparse matrix decomposition. *IEEE Trans. Image Process.* **2019**, *29*, 44–56. [[CrossRef](#)] [[PubMed](#)]
31. Chang, Y.; Yan, L.; Wu, T.; Zhong, S. Remote sensing image stripe noise removal: From image decomposition perspective. *IEEE Trans. Geosci. Remote. Sens.* **2016**, *54*, 7018–7031. [[CrossRef](#)]

32. Mújica-Vargas, D.; Gallegos-Funes, F.J.; de Jesús Rubio, J.; Pacheco, J. Impulsive noise filtering using a Median Redescending M-Estimator. *Intell. Data Anal.* **2017**, *21*, 739–754. [CrossRef]
33. Mújica-Vargas, D.; Rendón-Castro, A.; Matuz-Cruz, M.; Garcia-Aquino, C. Multi-core Median Redescending M-Estimator for Impulsive Denoising in Color Images. In *Mexican Conference on Pattern Recognition*; Springer: Cham, Switzerland, 2021; pp. 261–271.
34. Peter, D.J.; Govindan, V.; Mathew, A.T. Nonlocal-means image denoising technique using robust M-estimator. *J. Comput. Sci. Technol.* **2010**, *25*, 623–631. [CrossRef]
35. Wang, Z.; Bovik, A.C.; Sheikh, H.R.; Simoncelli, E.P. Image quality assessment: From error visibility to structural similarity. *IEEE Trans. Image Process.* **2004**, *13*, 600–612.
36. Rafael, C.G.; Richard, E.W. *Digital Image Processing Using MATLAB*; Pearson Education: Delhi, India, 2004.
37. Farcomeni, A.; Greco, L. *Robust Methods for Data Reduction*; CRC Press: Boca Raton, FL, USA, 2016.
38. Pitas, I.; Venetsanopoulos, A.N. *Nonlinear Digital Filters: Principles and Applications*; Springer: Berlin/Heidelberg, Germany, 1990; Volume 84.
39. Huber, P.J. *Robust Statistics*; John Wiley & Sons: New York, NY, USA, 1981; Volume 523.
40. Hampel, F.R.; Ronchetti, E.M.; Rousseeuw, P.J.; Stahel, W.A. *Robust Statistics: The Approach Based on Influence Functions*; John Wiley & Sons: New York, NY, USA, 1986; Volume 196.
41. Frigui, H.; Krishnapuram, R. A robust algorithm for automatic extraction of an unknown number of clusters from noisy data. *Pattern Recognit. Lett.* **1996**, *17*, 1223–1232. [CrossRef]
42. Kumar, V.V.; Nanalya, G. Removal of salt and pepper noise using robust M-filter. In Proceedings of the 2016 International Conference on Advanced Communication Control and Computing Technologies (ICACCCT), Ramanathapuram, India, 25–27 May 2016; pp. 175–178.
43. Ullah, I.; Qadir, M.F.; Ali, A. Insha’s redescending M-estimator for robust regression: A comparative study. *Pak. J. Stat. Oper. Res.* **2006**, *2*, 135–144. [CrossRef]
44. Chen, J.; Benesty, J.; Huang, Y.; Doclo, S. New insights into the noise reduction Wiener filter. *IEEE Trans. Audio, Speech Lang. Process.* **2006**, *14*, 1218–1234. [CrossRef]
45. FUJIFILM Healthcare Europe. Ultrasound Cases Info. 2020. Available online: <https://www.ultrasoundcases.info/> (accessed on 11 November 2022).
46. Suckling. The miniMIAS Database of Mammograms. 2017. Available online: <https://www.kaggle.com/kmader/mias-mammography> (accessed on 22 November 2020).
47. Jhon Beltran. Xrays Chest 224 small Aug Less Values Selected. 2018. Available online: <https://www.kaggle.com/jbeltranleon/xrays-chest-224-small-aug-less-values-selected> (accessed on 22 November 2020).
48. Buades, A.; Coll, B.; Morel, J.M. A non-local algorithm for image denoising. In Proceedings of the 2005 IEEE Computer Society Conference on Computer Vision and Pattern Recognition (CVPR’05), San Diego, CA, USA, 20–25 June 2005; Volume 2, pp. 60–65.
49. Immerkaer, J. Fast noise variance estimation. *Comput. Vis. Image Underst.* **1996**, *64*, 300–302. [CrossRef]
50. Perona, P.; Malik, J. Scale-space and edge detection using anisotropic diffusion. *IEEE Trans. Pattern Anal. Mach. Intell.* **1990**, *12*, 629–639. [CrossRef]
51. Tsiotsios, C.; Petrou, M. On the choice of the parameters for anisotropic diffusion in image processing. *Pattern Recognit.* **2013**, *46*, 1369–1381. [CrossRef]
52. Mújica-Vargas, D.; de Jesús Rubio, J.; Kinani, J.M.V.; Gallegos-Funes, F.J. An efficient nonlinear approach for removing fixed-value impulse noise from grayscale images. *J. Real-Time Image Process.* **2018**, *14*, 617–633. [CrossRef]
53. Wang, Z.; Simoncelli, E.P.; Bovik, A.C. Multiscale structural similarity for image quality assessment. In Proceedings of the The Thirty-Seventh Asilomar Conference on Signals, Systems & Computers, Pacific Grove, CA, USA, 9–12 November 2003; Volume 2, pp. 1398–1402.
54. Martin, D.; Fowlkes, C.; Tal, D.; Malik, J. A database of human segmented natural images and its application to evaluating segmentation algorithms and measuring ecological statistics. In Proceedings of the Eighth IEEE International Conference on Computer Vision, ICCV 2001, Vancouver, BC, Canada, 7–14 July 2001; Volume 2, pp. 416–423.
55. Al-Dhabyani, W.; Goma, M.; Khaled, H.; Fahmy, A. Dataset of breast ultrasound images. *Data Brief* **2019**, *28*, 104863. [CrossRef] [PubMed]
56. Franzen, R. Kodak Lossless True Color Image Suite. Available online: <https://r0k.us/graphics/kodak/> (accessed on 10 January 2023).

**Disclaimer/Publisher’s Note:** The statements, opinions and data contained in all publications are solely those of the individual author(s) and contributor(s) and not of MDPI and/or the editor(s). MDPI and/or the editor(s) disclaim responsibility for any injury to people or property resulting from any ideas, methods, instructions or products referred to in the content.